Ocean Engineering xxx (xxxx) xxx–xxx

Contents lists available at ScienceDirect

Ocean Engineering

journal homepage: www.elsevier.com/locate/oceaneng

Hydrodynamic analysis of a ducted, open centre tidal stream turbine using blade element momentum theory

Steven Allsop[a,b,c,*], Christophe Peyrard[b,c], Philipp R. Thies[d], Evangelos Boulougouris[e], Gareth P. Harrison[f]

[a] Industrial Doctoral Centre for Offshore Renewable Energy (IDCORE), University of Edinburgh, EH93LJ, UK
[b] EDF R & D – Electricité de France Research and Development (EDF R & D), LNHE, 6 Quai Watier, 78400 Chatou, France
[c] Saint-Venant Hydraulics Laboratory, Université Paris-Est, 6 quai Watier, 78400 Chatou, France
[d] College of Engineering, Mathematics and Physical Sciences, Renewable Energy Group, University of Exeter, TR109FE, UK
[e] Department of Naval Architecture, Ocean and Marine Engineering, University of Strathclyde, Glasgow G40LZ, UK
[f] Institute for Energy Systems, School of Engineering, University of Edinburgh, King's Buildings, Edinburgh EH93JL, UK

ARTICLE INFO

Keywords:
Tidal stream turbine
Marine current turbine
Ducted
Bidirectional
Open centre
Blade element momentum

ABSTRACT

This paper analyses two different configurations of horizontal axis Tidal Stream Turbines (TSTs) using a Blade Element Momentum Theory (BEMT) model. Initially, a 'conventional' three bladed and bare turbine is assessed, comparing against experimental measurements and existing literature. Excellent agreement is seen, increasing confidence in both the implementation of the theory and the applicability of the method. The focus of the paper lies on the analysis of a ducted and open centre turbine. An analytical adjustment to the BEMT model is applied, using empirical expressions detailed in the literature which are devised from Computational Fluid Dynamics (CFD) studies. This is modified to a symmetrical duct profile, calibrating certain geometrical parameters against blade resolved CFD studies of a bi-directional device. The results are validated with a coupled CFD blade element model (RANS BEM), where both models align very closely (within 2%) for most tip speed ratios (TSRs), including the peak power condition. Over predictions are seen at higher TSRs of up to 25% in power and 13% in thrust at TSR = 5, due to model limitations in replicating fully the complex flow interactions around the hub and the open centre. The presented approach benefits from significantly lower computational requirements, several orders of magnitude lower than reported in the RANS-BEM case, allowing practicable engineering assessments of turbine performance and reliability.

1. Introduction

Tidal Stream Turbine (TST) technology has been in the early stage developmental phase for a number of years, as engineering challenges in designing for extreme operating environments, combined with political and environmental factors has limited the rate of maturity. One of the earliest landmark projects was the MCT SeaGen, a 1.2 MW twin rotor device installed in the Strangford Loch, Northern Ireland in 2008, due to be decommissioned this year after generating 10 GW h electricity (ReNews, 2016). Despite hindrances in the industry, recent progression has led to the deployment of full scale arrays around the UK and France. Although there are many designs of tidal energy converters, the industry appears to have converged upon two configurations, which have seen the furthest advancement to date in terms of commercial scale deployment.

The first is a 'classical', 3 bladed horizontal axis design, similar to its wind turbine counterpart. The MeyGen project phase 1A (MeyGen, 2016) has seen the installation of its first three turbines of a 6 MW array as of January 2017 in the Pentland Firth, Scotland (shown in Fig. 1-1).

The second is a high solidity, ducted and open-centre turbine design. Ducts are primarily designed to increase the power extraction by increasing the mass flow rate through the rotor. Additional benefits include aligning yawed flow, providing a housing for a direct drive rim generator and removing the requirement for mechanical systems such as a gearbox. DCNS/OpenHydro have installed a pair of 500 kW rated capacity turbines (shown in Fig. 1-2), as a demonstration array in Paimpol-Bréhat, Northern France, in collaboration with EDF.

Hydrodynamic assessments are performed in order to gain insight into various aspects of the turbine. An extensive range of numerical models exist, each designed to perform different tasks and selected depending on the area of interest or objective of the study. Highly

* Corresponding author at: Industrial Doctoral Centre for Offshore Renewable Energy (IDCORE), University of Edinburgh, EH93LJ, UK.
E-mail addresses: steven-externe.allsop@edf.fr, s.allsop@ed.ac.uk (S. Allsop).

http://dx.doi.org/10.1016/j.oceaneng.2017.06.040
Received 29 January 2017; Received in revised form 13 June 2017; Accepted 17 June 2017

Fig. 1-1. Andritz Hydro Hammerfest 1.5 MW rated TST with installation into the Pentland Firth, Scotland (images credit: Atlantis Resources Ltd.) as part of the MeyGen Phase 1A deployment.

complex, high fidelity models are commonly used in design refinement, or to perform detailed assessments of turbine components under specific operating conditions. These can also be used to determine wake formation to measure the impact of the turbines on the tidal flow, as well as to describe the interactions of multiple turbines in an array.

Simpler models employ a more basic approach which are able to compute the force distributions along the rotor blades, and determine the overall performance of a turbine, aiding early stage decision making on optimal device designs for specific sites. Significantly lower computational requirements and fast processing time can be exploited for engineering applications where many analyses are required, such as performing numerous design iterations, analysing multiple or varying inflow conditions, or assessing fatigue loading.

Several industrial and academic codes are based on BEMT, (Batten et al., 2007; Masters et al., 2011; DNV GL Garrad Hassan, 2012) among which is a commercial standard software tool, 'Tidal Bladed', by the classification society DNV-GL. Despite the simplified approach, these models are well established and reliable, based on experience from the wind turbine industry. The BEMT code developed in this study is initially applied to a bare, 3-bladed turbine, where a full validation study is detailed in Allsop et al. (2016). However, the availability of such models for ducted, high solidity and open centre turbines is limited. At present, these types of devices are analysed using blade resolved CFD, which has a high computational requirement and is therefore not practical for multiple calculation applications. Less computationally intensive alternatives have been applied (Fleming et al., 2011; Turnock et al., 2011; Belloni et al., 2016) based on a coupled Reynolds Averaged Navier Stokes with blade element momentum (RANS-BEM), where case studies report good comparison with fully blade resolved studies, at a fraction of the processing time (McIntosh et al., 2012).

This paper aims to assess the performance of an analytical/empirical methodology to account for the presence of a duct, which is implemented within a BEMT code. This ducted BEMT model is applied to a bi-directional ducted turbine and results are compared with those of a coupled RANS BEM simulation.

The remainder of this paper is structured into 5 main sections: i) a brief outline of the underlying theory considered in the model; ii) the setup and implementation of the numerical model; iii) main results for the three bladed and ducted, open centre turbine; iv) a discussion comparing the different numerical models and implications as well as v) a conclusion of the main findings and recommendations for further work.

2. Methodology

The principles of BEMT are well defined in the literature, where this section aims to give a brief outline of the methodology. For further details and full derivations, the reader is referred to the following texts (Burton et al., 2011; DNV GL Garrad Hassan, 2012; Moriarty and Hansen, 2005).

Section 2.1 describes the BEMT model for a classical 3 bladed, bare turbine, with Section 2.2 outlining the adaptations based on an analytical framework to account for the presence of a duct. Section 2.3 defines output parameters that are used to validate the two models, with Sections 2.4 and 2.5 defining various correction factors in order to account for physical occurrences that are neglected in the BEMT.

2.1. Blade element momentum theory

One-dimensional momentum theory models the turbine as an infinitely thin, semi-permeable actuator disc exerting zero friction,

Fig. 1-2. DCNS/OpenHydro 500 kW rated turbine with installation at the Paimpol Bréhat site, Northern France (images credit: DCNS/OpenHydro).

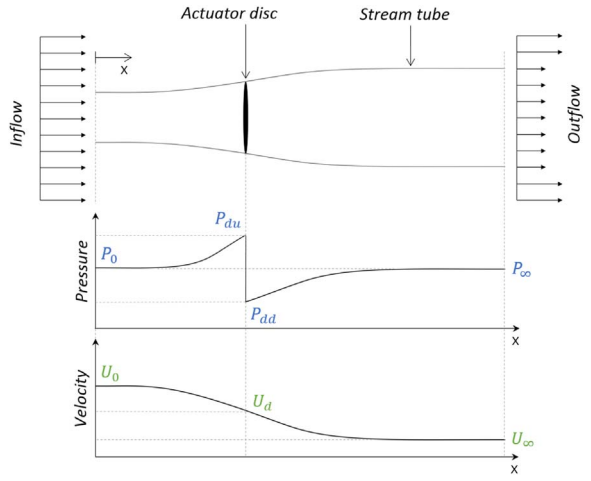

Fig. 2-1. Schematic of the actuator disc model within a stream-tube, showing a representation of axial changes in pressure and velocity.

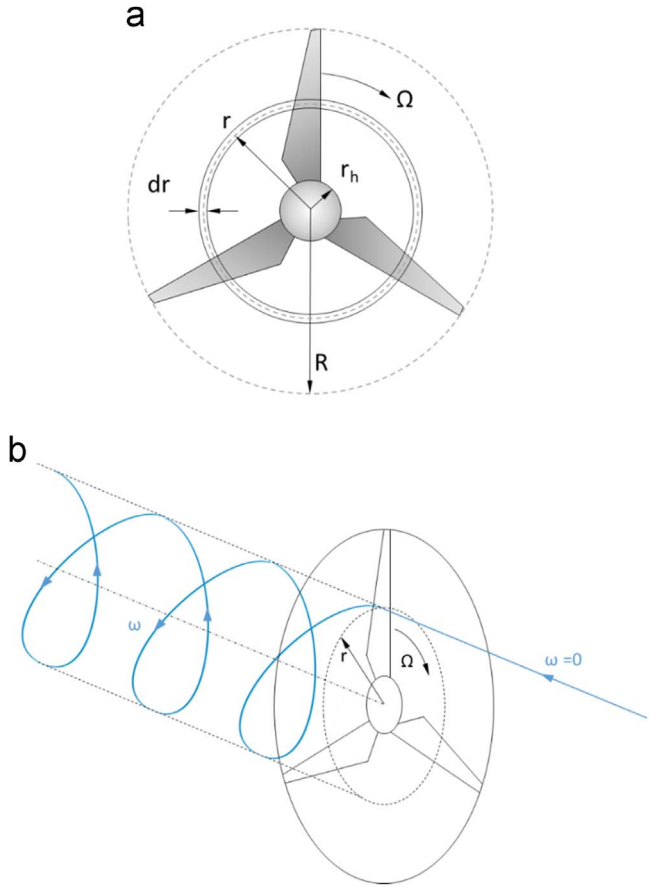

Fig. 2-2. a) split of rotor disc into annular rings compared to overall turbine geometry (top) b) depiction of a particle interacting with rotor showing changes in rotational velocity (bottom).

bounded by a stream-tube (Fig. 2-1). Flow velocities and pressures at various locations along this control volume can be related using continuity and Bernoulli's equations. The axial force (thrust) on the disc as a result of the change in pressure can be equated to the change in axial momentum. The disc is split into a number of discrete annular rings as shown in Fig. 2-2a, assuming the momentum is extracted only from fluid passing through each individual ring. The pressure/momentum balance can be applied independently to each ring such that:

$$dT = 4\pi\rho U_0^2 a(1-a)rdr \tag{1}$$

where: $a = (U_0 - U_d)/U_0 = (U_0 - U_\infty)/2U_0$ is the axial induction factor, dT is the element thrust (N), ρ is the fluid density (kg m^{-3}), U_0 is the reference upstream velocity (m s^{-1}), U_d is the flow velocity at the disc (m s^{-1}), r *is* the local element mean radius (m) and dr is the radial length of each ring (m).

Associated with the change in axial momentum of the fluid as a result of the presence of the disc is also a change in angular momentum as a result of the turbine rotation. The fluid entering the turbine is considered straight, with zero rotational motion. The fluid passing through the rotating disc exerts a torque on the rotor, which requires an equal and opposite torque imposed on the fluid. This reaction torque causes the fluid to rotate in an opposite direction to turbine rotation. This has an associated gain in angular momentum, as the wake flow now has a velocity component tangential to the rotation (see Fig. 2-2b). This increase in angular momentum can be related to the torque of each annular ring as a function of the tangential velocity and radial position:

$$dQ = 4\pi\rho a'\Omega U_0(1-a)r^3dr \tag{2}$$

where: $a' = \omega/2\Omega$ is the tangential induction factor which expresses the change in tangential velocity, dQ is the element torque (N m), ω the angular velocity of the wake (rad s^{-1}) and Ω the angular velocity of the turbine (rad s^{-1}).

Blade element theory divides the blade into a number of discrete hydrofoil sections, which are analysed two dimensionally, neglecting any span-wise (radial) interactions. The flow at each 2D element has associated axial and tangential components of velocity, with the inflow angle (ϕ) located between (see Fig. 2-3). The aerodynamic lift and drag forces on the blade element act parallel and perpendicular to this inflow angle, and can be determined using the standard aerofoil equations for lift and drag (DNV GL Garrad Hassan, 2012):

$$dL = \frac{1}{2}C_L\rho W^2 c dr, \tag{3}$$

$$dD = \frac{1}{2}C_D\rho W^2 c dr, \tag{4}$$

where W is the resultant fluid velocity (m s^{-1}) and c the blade chord (m). Coefficients of lift (C_L) and drag (C_D) are input from two dimensional aerofoil data as a function of angle of attack (α), which can be determined from the inflow angle (ϕ) and the geometrical twist

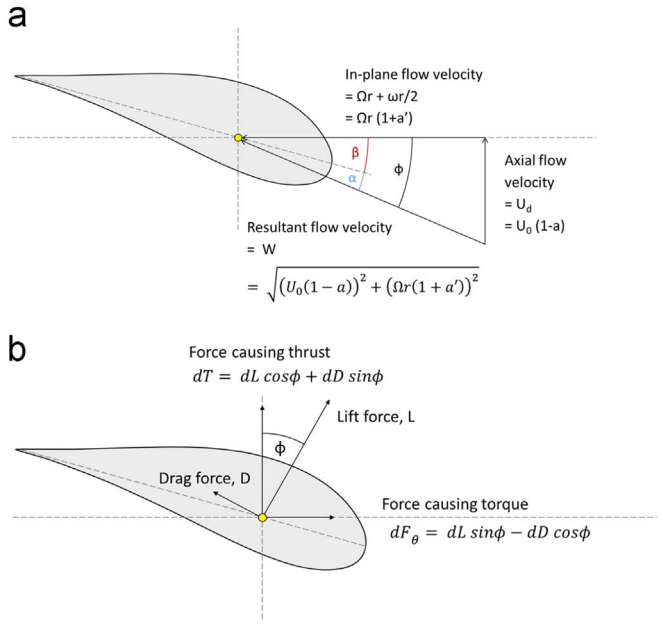

Fig. 2-3. a) Blade element flow velocity vectors (top) b) Blade element forces as a function of the aerodynamic forces and inflow angle (bottom).

down the blade length (β). The forces causing thrust and torque can then be resolved trigonometrically, where B is the number of blades:

$$dT = \frac{1}{2}\rho W^2 Bc\,(C_L cos\phi + C_D sin\phi)\,dr, \tag{5}$$

$$dQ = \frac{1}{2}\rho W^2 Bc\,(C_L sin\phi - C_D cos\phi)\,r dr, \tag{6}$$

BEMT assumes that the change in momentum of each annular ring is solely accountable from the hydrodynamic forces on the corresponding blade elements (Burton et al., 2011). Hence the axial and tangential force equations from each theory are equated, giving expressions for calculating axial and tangential induction factors:

$$\frac{a}{(1-a)} = \frac{\sigma_r (C_L \cos\phi + C_D \sin\phi)}{4\sin^2\phi}, \tag{7}$$

$$\frac{a'}{(1+a')} = \frac{\sigma_r (C_L \sin\phi - C_D \cos\phi)}{4\sin\phi\cos\phi}, \tag{8}$$

where $\sigma_r = Bc/2\pi r$ is the local blade solidity. As the aerofoil coefficients vary non-linearly with angle of attack, these equations must be solved iteratively.

As the method neglects radial interactions, and considers only flow in the control volume, the approach is limited when considering physical phenomena such as vortex shedding and mixing with free stream fluid. Various correction factors can be applied to Eqs. (7) and (8) to account for these effects, which are described in Sections 2.4 and 2.5.

2.2. Ducted BEMT

The incorporation of a duct aims to direct more flow through the turbine, and hence increase the momentum available for extraction. This is achieved by forcing of expansion in the diffuser reduces the pressure downstream, which augments the flow at the throat and results in a higher mass flow rate. The presence of the structure alters the flow profile as shown in Fig. 2-4, which makes the momentum equations based on the previous stream tube assumption unsuitable.

The effects of the duct can be categorised by four main factors: i) the diffuser ratio (ratio of outlet area to throat area); ii) the flow separation within the diffuser; iii) the back pressure reduction at the exit and iv) the associated viscous losses (van Bussel, 2007).

An analytical model devised by Lawn (2003) relates the change in velocity using Bernoulli's equations to the change in pressure at various locations along the streamtube. These can be expressed in terms of the inlet efficiency (η_{02}), diffuser efficiency (η_{34}) and base pressure coefficient ($C_{p,b}$) by the following:

$$\eta_{02} = \frac{p_2 - p_0}{\frac{1}{2}\rho(U_0^2 - U_2^2)}, \tag{9}$$

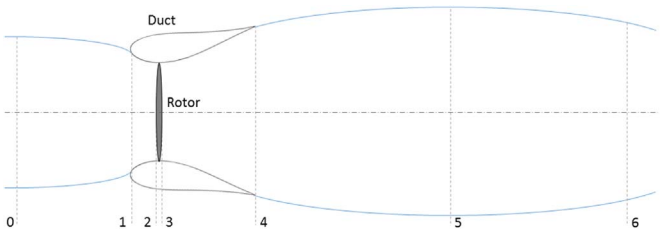

Fig. 2-4. Schematic of ducted turbine incorporating the actuator disc bounded by a stream tube, with numbers corresponding to sections in which areas, pressures and velocities are taken, consisting of: 0 – inflow upstream; 1 – duct inlet; 2 – actuator disc upstream; 3 – actuator disc downstream; 4 – duct outlet; 5 – wake downstream; 6 – wake far downstream.

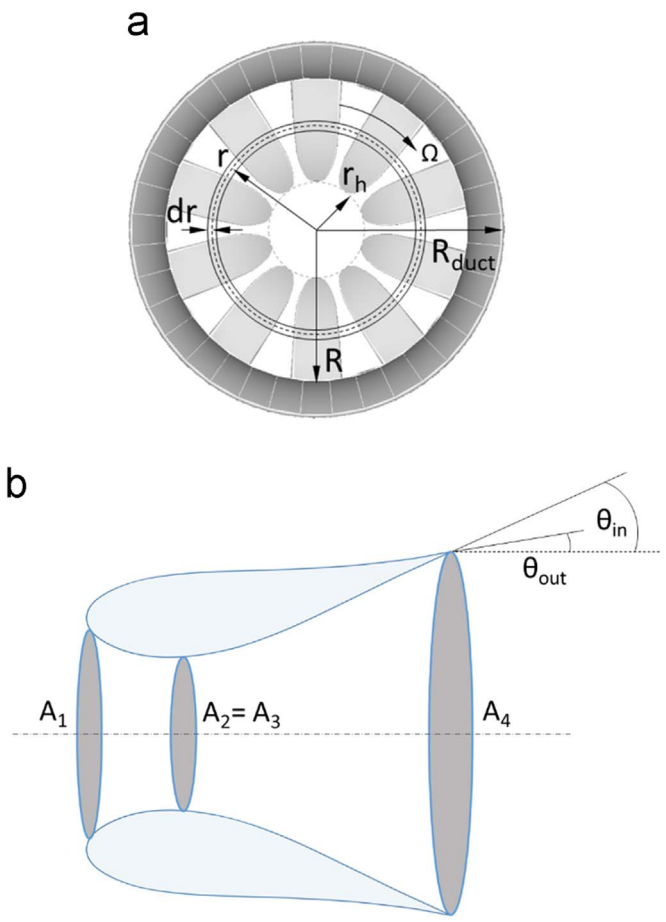

Fig. 2-5. Fig. 2 5 Ducted turbine a) rotor split into annular rings (top) and b) definition of geometrical parameters (bottom).

$$\eta_{34} = \frac{p_4 - p_3}{\frac{1}{2}\rho U_3^2\left(1 - \frac{A_3^2}{A_4^2}\right)}, \tag{10}$$

$$C_{p,b} = \frac{p_0 - p_4}{\frac{1}{2}\rho U_0^2}, \tag{11}$$

Experimental measurements or CFD results are then required to solve these equations. This framework is adopted by Shives and Crawford (2011), where efficiencies are quantified using RANS simulations incorporating an actuator disc representation of the rotor. Several geometries of unidirectional ducts are analysed based on NACA0015 aerofoil shapes (Abbott and Von Doenhoff, 1959), with varying geometrical parameters of: inlet contraction ratio (A_1/A_3); the diffuser expansion ratio (A_4/A_3); inner and outer diffuser surface angles (θ_{in} and θ_{out}), as shown in Fig. 2-5.

Empirical approximations of the analytical expressions are then derived by Shives and Crawford (2011), based on the CFD results. The inlet efficiency (η_{02}) was found to be within 5% of unity for all geometries considered, and therefore taking an efficiency of 100% was considered to have a negligible effect on the overall rotor forces. The diffuser efficiency can be written in terms of duct geometry, to characterise flow separation within the duct:

$$\eta_{34} = a_1 + b_1\left(\frac{A_3}{A_4}\right) + c_1\theta_{in} + d_1\left(\frac{A_1}{A_2}\right) \tag{12}$$

where $A_i = \pi R_i^2$ is the area at various positions along the stream tube (m^2). Similarly, the base pressure coefficient caused by obstruction of the flow is determined by:

Table 2-1
Coefficients for empirical expressions of diffuser efficiency and base pressure coefficient, from Shives and Crawford (2011).

a_1	b_1	c_1	d_1	a_2	b_2	c_2	d_2	e_2	f_2
0.8867	0.5212	−0.0108	−0.1313	0.2701	−0.333	0.0269	0.1068	−0.0152	−0.1275

$$C_{p,b} = a_2 + b_2\left(\frac{A_3}{A_4}\right) + c_2\theta_{out} + (d_2 + e_2\theta_{out})C_T + f_2 C_T^2 \tag{13}$$

where all coefficients are found using a least squares optimisation, summarised in Table 2-1.

The pressure change through the diffuser can be defined using the continuity equations, such that the coefficient of pressure between positions 3 and 4 can be written:

$$C_{p,34} = \frac{p_4 - p_3}{\frac{1}{2}\rho U_3^2} = \eta_{34}\left(1 - \frac{A_3^2}{A_4^2}\right) \tag{14}$$

And the axial induction factor can finally be calculated using the following equation, where wake swirl is neglected:

$$1 - a = \sqrt{\frac{\eta_{02} - C_{Ti} + C_{p,b}}{\eta_{02} - C_{p,34}}} \tag{15}$$

The empirical/analytical model is validated against power and thrust curves generated with CFD on three additional validation duct geometries, where reasonable agreement is seen.

2.3. Rotor power and thrust

Once axial and tangential induction factors are converged, coefficients of power (C_P) and trust (C_T) for the rotor are calculated to present non-dimensionalised turbine properties for comparative studies. These are often presented as a variation against the tip speed ratio (TSR), defined as:

$$C_T = \frac{\sum_{r_{hub}}^{R} dT}{\frac{1}{2}\rho A U_0^2}, \tag{16}$$

$$C_P = \frac{\sum_{r_{hub}}^{R} dQ\Omega}{\frac{1}{2}\rho A U_0^3}, \tag{17}$$

$$TSR = \frac{\Omega R}{U_0}, \tag{18}$$

where $A = \pi R^2$ is the area of the disc (m^2), or $A = \pi R_{duct}^2$ in the case of the ducted turbine.

Comparisons of bare and ducted turbines have previously been assessed using the rotor diameter (Hansen, 2008). In order to fairly compare the same relative areas, the RANS BEM study takes the area at the duct inlet, and neglects the open centre, as explained by Belloni et al. (2016). Although this is not the objective of the present study, these definitions are used in order to gain directly comparable results for validation. The tip speed ratio is defined in all cases using the rotational velocity at the outer radius of the rotor, despite the fact that the blades are connected at either end in the ducted case. In addition, the thrust coefficient at the local elements can be calculated as:

$$C_{T,loc} = \frac{T}{\frac{1}{2}\rho A_{rotor} U_d^2} \tag{19}$$

2.4. Tip and hub losses

Radial movement of fluid occurs at the blade tips and at the hub, as it is drawn from the pressure to the suction side of the rotor. Due to the 2-dimensional nature of the blade element and momentum methods, this movement is not accounted for directly in the theory and therefore has to be included through an alternative method. Although exact solutions such as proposed by Bessel and Biot-Savart, the issues arise with integrating into the BEMT method (Burton et al., 2011). The Prandtl approximation solution yields a relatively simple analytical function which has been previously employed to account for the effects of the tip losses (Chapman et al., 2013), and is easily implemented into BEMT. Flow shedding at the blade tips leads to rotating helical structures in the wake, which Prandtl conceptualises as a succession of discs travelling at a velocity between the free stream and the wake (Burton et al., 2011). The loss factor can approximate the reduction in hydrodynamic efficiency at the tip, and be expressed in the closed solution form proposed by Prandtl:

$$F_{tip} = \frac{2}{\pi} cos^{-1}\, e^{-f_{tip}} \tag{20}$$

where the tip exponential term can be expressed:

$$f_{tip} = \pi\left(\frac{R_w - r}{d}\right) \tag{21}$$

where $R_W - r$ is the distance from the wake edge and d is the normal distance between successive vortex sheets. This distance is related to the flow angle ϕ_s and the number of vortex sheets intertwining from B number of blades:

$$d = \frac{2\pi R_w}{B}\sin\phi_s = \frac{2\pi R_w}{B}\frac{U_0(1-a)}{W_s} \tag{22}$$

Taking the resultant wake velocity $W_S = \sqrt{(U_0(1-a))^2 + (\Omega r)^2}$ and taking the Glaeurt adjustment such that $\frac{R_w}{W_s} \approx \frac{r}{W}$ (Masters et al., 2011):

$$F_{tip} = \frac{2}{\pi} cos^{-1}\, e^{-\frac{B}{2}\frac{R-r}{r}\frac{1}{\sin\phi}} \tag{23}$$

A similar expression is also suggested to account for losses at the hub (Moriarty and Hansen, 2005):

$$F_{hub} = \frac{2}{\pi} cos^{-1}\, e^{-\frac{B}{2}\frac{r-r_h}{r_h}\frac{1}{\sin\phi}} \tag{24}$$

These can then be combined as an overall loss correction factor defined by:

$$F = F_{tip} F_{hub} \tag{25}$$

The combined tip/ hub loss factor can then be input directly as a multiplication factor into the expressions (Chapman et al., 2013) for thrust and torque from momentum theory (Eq. (1) and Eq. (2)) such that:

$$dT = 4\pi\rho U_0^2 a(1-a) r dr \boldsymbol{F}, \tag{26}$$

$$dQ = 4\pi\rho a' \Omega U_0 (1-a) r^3 dr \boldsymbol{F} \tag{27}$$

Axial and tangential forces from blade element theory are derived from aerodynamics equations, so remain unchanged.

2.5. Highly loaded conditions

At high axial induction factors, thrust forces are under predicted by the momentum equations as the stream tube representation does not account for interactions with the free stream fluid. For $a > 0.5$ an unphysical reversal of flow in the wake is seen, from: $U_\infty = U_0(1-2a)$. In reality, turbulent mixing occurs with the free stream flow, injecting momentum into the slow moving fluid behind the turbine. Physical

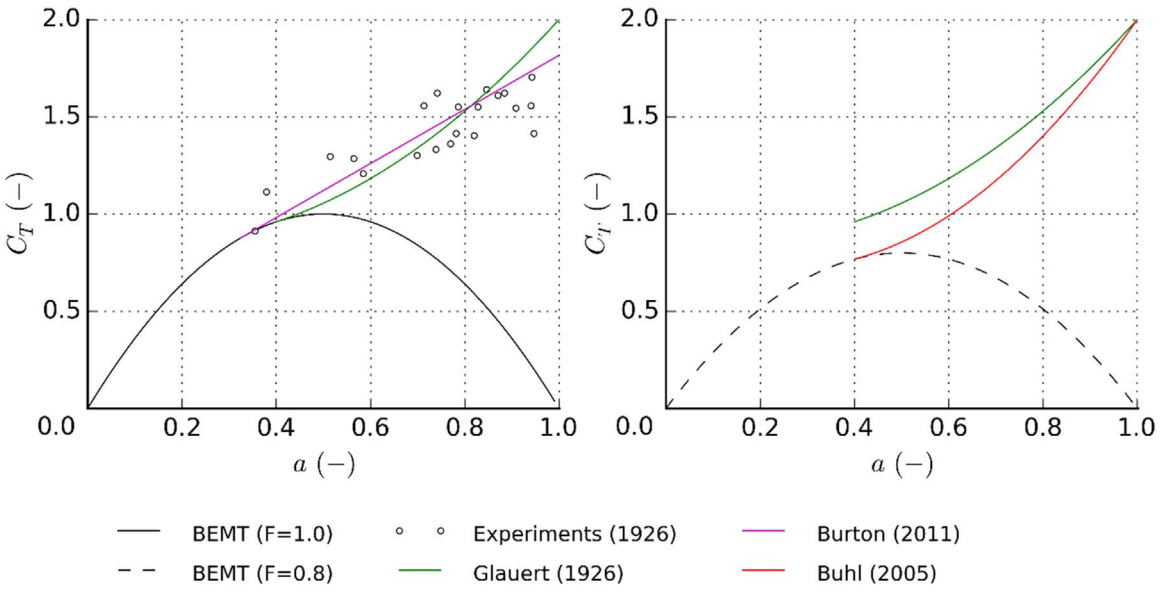

Fig. 2-6. Thrust coefficient against axial induction factor, showing comparisons against BEMT with a) experimental values (points) and semi-empirical corrected values (left) and b) highly loaded corrected values with an arbitrary tip/hub loss of 0.8 applied (right).

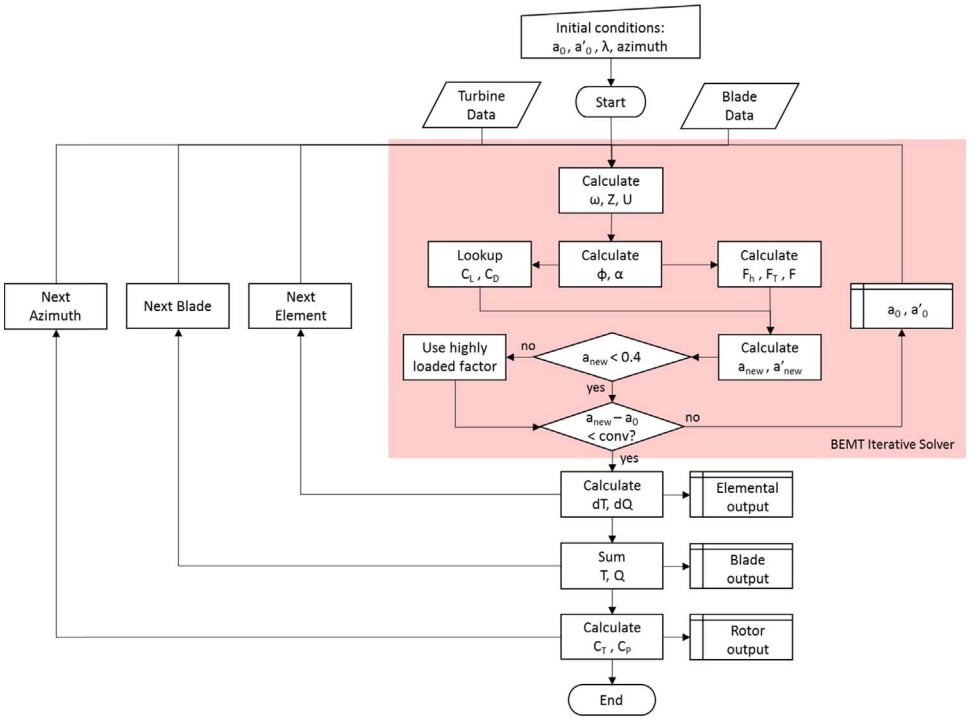

Fig. 3-1. General BEMT code structure implemented in Python.

experiments with flat plates carried out by Glauert have shown much higher thrusts at axial induction factors above 0.4, as shown in Fig. 2-6a.

Various best line fits to this data have been proposed, including a parabola proposed by Glauert (Burton et al., 2011) such that:

$$\text{For} a \leq 0.4 : C_T = 4a(1-a) \tag{28}$$

$$\text{For} a > 0.4 : C_T = 0.889 - \frac{0.0203-(a-0.143)^2}{0.6427} \tag{29}$$

However, when combined with the tip/hub loss correction factor, a numerical instability occurs due to a gap at transition to the highly loaded regime (see Fig. 2-6b). A solution as devised by Buhl (2005) has previously successfully been implemented into BEMT (Chapman et al., 2013), which yields a smooth transition from the Glauert parabola to the prediction based on the axial momentum equations. Buhl reported reasonable agreement with the experimental data, as well as fixed boundary condition at a = 1, analogous to a solid plate fully impeding flow.

$$\text{For } a \leq 0.4 : C_T = 4Fa(1-a) \tag{30}$$

$$\text{For } a > 0.4 : C_T = \frac{8}{9} + \left(4F - \frac{40}{9}\right)a + \left(\frac{50}{9} - 4F\right)a^2 \tag{31}$$

As these are relating to the overall rotor, we can implement this back to the momentum equations to write expressions for each annular ring as:

$$\text{For } a \le 0.4 : dT = 4\pi\rho U_0^2 a(1-a) r dr F$$
$$\text{For } a > 0.4 : dT = \pi\rho U_0^2 \left(\frac{8}{9} + \left(4F - \frac{40}{9}\right)a + \left(\frac{50}{9} - 4F\right)a^2\right) r dr \quad (32)$$

3. Model setup and input definitions

This section addresses the implementation of the BEMT into the code and defines the various input data for the validation cases. Sections 3.1 and 3.2 describe the BEMT code structure for the conventional, 3-bladed case and the ducted open centre case respectively. Sections 3.3 and 3.4 detail the process of generating aerofoil coefficients, followed by the definition of other input parameters for the conventional and ducted validation cases in Sections 3.5 and 3.6 respectively.

3.1. Numerical implementation

The BEMT equations are solved iteratively with a programme written in Python. The overall code structure that has been utilised in the work presented in this paper is shown in Fig. 3-1.

Here the convergence shown is based purely on the axial induction factor, however this is improved to include both axial and tangential induction factors in the convergence criteria. The iterations are performed using a minimisation package, an objective function similar to that of *fmincon* within Matlab, used in other codes (Masters et al., 2011; Shives, 2011). The thrust and torque from each theory is considered equal, therefore the values from momentum and blade element can be rearranged and summed to equal the minimisation value (g):

$$g = (dT_1 - dT_2)^2 + (dQ_1 - dQ_2)^2 \quad (33)$$

To implement the highly loaded condition:

$$\text{For } a \le 0.4:$$
$$g = \left(4\pi U_0^2 a(1-a) r F - \frac{1}{2} W^2 Bc (C_L cos\phi + C_D sin\phi)\right)^2 + \left(4\pi a' \Omega U_0 (1-a) r^2 F - \frac{1}{2} W^2 Bc (C_L sin\phi - C_D cos\phi)\right)^2 \quad (34)$$

$$\text{For } a > 0.4:$$
$$g = \left(\pi U_0^2 r \left(\frac{8}{9} + \left(4F - \frac{40}{9}\right)a + \left(\frac{50}{9} - 4F\right)a^2\right) - \frac{1}{2} W^2 Bc (C_L cos\phi + C_D sin\phi)\right)^2 + \left(4\pi a' \Omega U_0 (1-a) r^2 F - \frac{1}{2} W^2 Bc (C_L sin\phi - C_D cos\phi)\right)^2 \quad (35)$$

where each part is squared to avoid convergence to an incorrect solution.

The *minimise* function within SciPy offers a variety of optimisation algorithms, which can be selected based on the nature of the problem (SciPy Community, 2016). In this case, the Sequential Least Squares Programming (SLSQP) gave the best compromise between running time, convergence and operational constraints. A maximum iteration limit was set to 1000, and a tolerance for the value g of 1.0E-10. Boundary constraints were set to ensure that induction factors stay within reasonable limits, where tangential values being less than 0.5, and axial between −0.9 and 0.9.

3.2. Duct model implementation

The same minimise objective function is applied, however the minimisation value is defined as:

$$g = ((\eta_{02} - CT_i + C_{pb} - (\eta_{02} - C_{P34})(1-a)^2)^4 + \left(4\pi a' \Omega U_0 (1-a) r^2 F - \frac{1}{2} W^2 Bc (C_L sin\phi - C_D cos\phi)\right)^4 \quad (36)$$

Here the highly loaded condition is not included, as the axial induction factor never converges on $a > 0.4$. The equation now incorporates the axial induction factor expression from the duct analytical/empirical model as defined in Eq. (15), and thrust coefficient C_{Ti} calculated from the blade element theory using Eq. (5). The thrust and torque sides are increased to the power 4 in this case, as it was discovered to have a higher stability. The iterative loop steps through the induction factors searching for equilibrium between the momentum and blade element theories, in order to satisfy the minimisation condition *(g)*. The higher stability is thought to be achieved with the larger exponent value due to smaller increments imposed when the approaches the equilibrium value. This increases the number of steps taken to reach convergence, however does not noticeably affect the running time.

Where available, the duct geometry is taken directly from the reference Belloni et al. (2016), including duct inlet and outlet radii. The inlet and outlet diffuser surface angles required by the analytical model are not given, and not easily defined for a bi-directional ducts. A calibration study was thus performed to estimate appropriate values, by applying the model to a commercial open centre device, and comparing the corresponding thrust and power curves with blade resolved CFD simulations. Appropriate values were determined as: θ_{in} = 30° and θ_{out} = 10°.

Due to the configuration of blade tips being connected, the formation of tip vortices is restricted, which has implications on the tip-losses seen in classical turbines. CFD studies have reportedly shown that the change in axial velocity at the tip is small (Fleming and Willden, 2016) and therefore the tip loss factor is set to unity.

For this case, an open centre hub is incorporated, connecting the ends of the blades at the centre. This is thought to constrain the vortex shedding which is the basis of the Glauert hub loss, and therefore is assumed to be unity in this case. This is a limitation of the model, as the complex nature of the flow in this region is thought to have associated 3 dimensional effects and therefore associated hydrodynamic efficiency losses. An alternative correction factor is currently being sought, however due to the additional complexity in the mixing with flow through the open centre, requires extensive blade resolved CFD studies.

3.3. Aerofoil coefficients

Aerofoil characteristics are required in determining the element aerodynamic forces, which can be obtained directly from catalogued data such as (Abbott and Von Doenhoff, 1959) which are based on wind tunnel experiments at specific Reynold's numbers. XFOIL is an alternative method: a Fortran based programme incorporating a linear vorticity function panel method with a viscous boundary layer and wake model (Drela, 1989). For NACA profiles not contained within the XFOIL database, surface ordinates are obtained from catalogued data (UIUC Applied Aerodynamics Group, 2015) and prescribed, along with the chord based Reynolds number as:

$$Re_{ch} = \frac{\rho c W}{\mu} \quad (37)$$

where $W = \sqrt{U_0^2 + (\Omega r)^2}$ denotes the resultant velocity over the surface of the aerofoil (m s^{-1}) and μ is the dynamic fluid viscosity (Nsm^{-2}). Small changes in Reynold's number were found to have an insignificant on the overall rotor performance, and therefore the rotational velocity is taken at the optimal performance of the turbine. As the Viterna extrapolation function uses chord and thickness values at 75% down the length of the blade (Ning, 2013), it seems reasonable to use the

same location in Reynolds number calculation.

Aerofoil coefficients for the bare 3-bladed turbine uses XFOIL generated data (at Re_{ch} = 3.0E + 05), whereas the ducted case takes catalogued data (at Re_{ch} = 1.5E + 06).

3.4. Corrections to aerofoil coefficients

As XFOIL calculations and experiments are based on 2D static wind tunnel measurements, the 3D nature of flow due to the rotation of the blade is not accounted for. In reality, radial forces in the fluid induce a Coriolis Effect, acting in the direction of the trailing edge which effectively delays the onset of boundary layer separation. This delayed stall phenomenon varies as a function of chord and radius, and can be accounted for by applying a Du-Selig (Tangler and Selig, 1997) model to the lift coefficients, and an Eggers (Hansen, 2004) adjustment to the drag.

As a result of BEMT iteratively solving for inflow angle, data for large range of angles of attack is required, in some cases exceeding the point of stall, which is beyond the capabilities of XFOIL. Values in these conditions can be generated using an extrapolation function as proposed by Viterna (Viterna and Janetzke, 1982), using the aerofoil aspect ratio 75% down the length of the blade.

3.5. Classical bare turbine properties

Validation of the classical BEMT model for bare turbines is performed against 1/20th scale model experiments (Batten et al., 2006). The 3-bladed turbine has a rotor radius (R) of 0.4 m, and tests are performed in a fully enclosed cavitation tunnel. Radial distribution of blade chord (c), thickness (t) and twist (β) are detailed in Table 3-1.

Three flow rates and blade pitches are considered, detailed in Table 3-2:

The flow through the water column under experimental conditions is inherently unsteady and non-uniform, combined with complex interactions with the surrounding walls. The blockage ratio of the experimental setup is 17%, and results are quoted by the author in their blockage corrected form (Bahaj et al., 2007). As tests are run in a cavitation tunnel, there are no free surface effects. Within the BEMT, the inflow is assumed as a steady and 'frozen', where in this analysis a shear profile is incorporated in order to approximate the effects of bottom friction as a 1/7th power law:

$$U_0 = U_{hub}\left(\frac{z}{z_{hub}}\right)^{\frac{1}{7}} \tag{38}$$

where U_{hub} is the average flow velocity at the hub height (m s^{-1}), z is the height of the element above the seabed (m) and z_{hub} is the height of the hub above bottom, taken as 0.6 m. z is calculated as a function of the blade azimuth and element radial location and inserted in the above equation to determine the inflow velocity for each element. This velocity is then used in the BEMT loop, where an azimuth stepping function is applied. Rotor power and thrust coefficients are then determined by taking the average axial and tangential forces over one turbine rotation.

Table 3-1
1/20th scale turbine properties showing distributions with normalised radius (Bahaj et al., 2007).

r/R	β (°)	c/R	t/c (%)
0.20	15.0	0.125	24.0
0.30	9.5	0.116	20.7
0.40	6.1	0.106	18.7
0.50	3.9	0.097	17.6
0.60	2.4	0.088	16.6
0.70	1.5	0.078	15.6
0.80	0.9	0.069	14.6
0.90	0.4	0.059	13.6
1.00	0.0	0.050	12.6

Table 3-2
1/20th scale model experimental case conditions (Bahaj et al., 2007).

Parameter	Case 1	Case 2	Case 3
Inflow velocity (m/s)	1.73	1.54	1.3
Blade pitch (°)	5	10	12

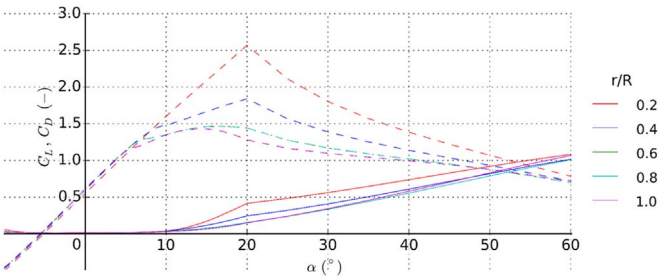

Fig. 3-2. Coefficient of lift (dashed lines) and drag (solid lines) against angle of attack for NACA63-8xx profiles for various normalised radii, at a Reynold's number 3.0E + 05.

The blade profile consists of NACA63-8xx aerofoil sections, xx being the thickness to chord ratio. The lift and drag coefficients against angle of attack for a Reynolds number of 3.0E + 05 (corresponding to 1.73 m s^{-1} inflow velocity) are shown in Fig. 3-2, generated using XFOIL. Values are 3D stall delay corrected as a function of location along the blade, and extrapolated past stall condition.

3.6. High solidity, ducted, open-centre turbine properties

To assess the performance of the duct BEMT model, comparisons are made against a coupled RANS BEM study of a bidirectional ducted and open centre turbine. This is based on full scale geometry, with general dimensions of duct radius (R_{duct}), rotor radius (R_{rotor}) and hub radius (R_{hub}) given in Fig. 3-3. Values of inlet and outlet angles (indicated in Fig. 2-5) are calibrated with the blade resolved CFD studies, where θ_{in} = 30° and θ_{out} = 10° show the best representation. A sensitivity analysis of these parameters is shown in Section 5.6.

The number of blades, aerofoil chord lengths and thicknesses are incorporated into values of solidity (σ_r), where radial distributions are detailed in Table 3-3.

One flow condition is considered, based on a uniform inflow with no bottom friction, at a constant velocity of 2 m s^{-1}. This has a corresponding chord based Reynolds number of approximately 1.0E + 06. The blades consist of Risø-A1-24 aerofoils, with lift and drag coefficients as shown in Fig. 3-4, taken from wind tunnel data at a Reynolds number of 1.6E + 06 (Fuglsang et al., 1999). These raw values are directly applied to the mode, with no 3D correction implemented, to be consistent with the validation methodology (Belloni, 2013). No extrapolation function is used, where if α < 5°, C_L and C_D are equal to those at α = 5°. Additionally, for α > 35°, C_L and C_D are equal to those at α = 35°.

4. Results

This section presents the results of the two BEMT models and compare them with various validation data from the literature. Section 4.1 gives the comparison of the conventional 3-bladed case with previous scale model experimental data. Sections 4.2 and 4.3 present the results of the ducted BEMT compared to a coupled RANS-BEM model, where overall rotor performance as well as span-wise variations are shown.

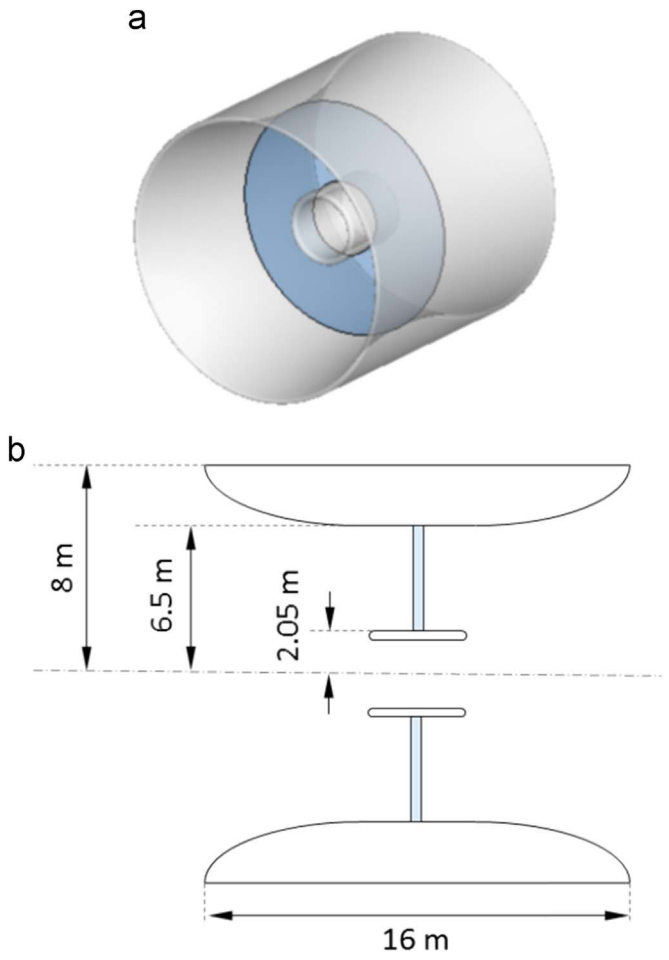

Fig. 3-3. Ducted open centre turbine overall dimensions (Belloni et al., 2016).

Table 3-3
Ducted and open centre turbine properties variation with normalised radius. Data reproduced from Belloni et al. (2016).

r/R	β (°)	σ_r
0.30	29.7	0.420
0.40	25.6	0.305
0.50	20.8	0.220
0.60	17.2	0.163
0.70	14.2	0.124
0.80	12.0	0.100
0.90	10.3	0.083
1.00	8.4	0.070

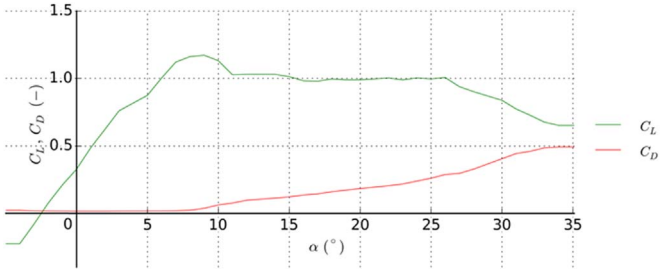

Fig. 3-4. Coefficients of lift and drag against angle of attack for Riso-A1-24 aerofoil under a Reynold's number 1.6E + 06 (Fuglsang et al., 1999).

4.1. Classical bare turbine validation

Using the described input data, the model is run for each individual inflow velocity and pitch. Intermediate calculation steps are inspected in order to assess the model performance, to ensure convergence is well established and to gain indications of magnitude and location at which correction factors are being applied. Fig. 4-1 shows the distribution of axial and tangential induction factors as well as the tip/hub loss correction factor along the blade length for an inflow velocity of 1.73 m s^{-1}. The axial induction factor is seen to exceed the transition to the highly loaded regime only at this inflow, occurring mainly at the blade tips except for at a TSR of 8. The tip/hub loss describes the reduction in hydrodynamic efficiency along the blade, becoming more influential towards the tip and hub as per its definition. The magnitude of this efficiency decreases with TSR, where the tip losses are clearly more significant in all cases considered. For the lowest TSRs, the correction can be seen to apply along the entire length of the blade.

Fig. 4-2 shows the power and thrust curves for the turbine, comparing measured and numerical data. Overall trends are similar for each inflow: levels generally increase to a peak at an optimal TSR, the largest corresponding to the highest inflow. For the most part, results from the BEMT models show excellent agreement with the experimental data. Inter comparison of the numerical models also shows very similar trends, with little divergence in the power at the lowest inflow velocity. Regions of over prediction in power are evident towards the higher TSRs. This is potentially caused by the large blockage correction factor applied to the experimental data.

4.2. Ducted rotor performance and thrust

The axial induction factor for all cases is found to be below the transition to the highly loaded regime for all TSR, so no highly loaded correction factor is applied.

Fig. 4-3 shows the coefficient of power and thrust, which again follows an increasing trend up to a maximum at an optimal TSR. Comparison of the ducted BEMT results with RANS-BEM shows exceptional agreement, particularly up to the optimal at 3.0. Beyond the peak, a divergence is seen between the datasets, where ducted BEMT calculates up 25% higher in power and 13% in thrust at TSR 5.

4.3. Ducted rotor blade distribution

Rotor averaged values give an overall indication to the performance of a turbine, however it is also important to be able to assess the force distributions along the blade length, particularly when performing loading and bending moments for structural assessments. Fig. 4-4 shows the blade distributions of certain parameters calculated in the model, namely the velocity at the disc, angle of attack and local element coefficient of thrust. Comparing the ducted BEMT to RANS-BEM, excellent agreement is seen for angles of attack at all TSRs considered, as well as for velocity and local element thrust up to TSR 3. Some discrepancies are evident when inspecting the velocity and local thrust at TSRs 4–5. This is in accordance with the results for the entire rotor, but here we can identify the divergences are located at blade elements towards the hub (for low r/R values).

5. Discussion

Here we discuss the findings from the results, with Section 5.1 focussing on the validation of the classical code with a conventional turbine and Section 5.2 on the ducted BEMT model. Additional observations, model limitations, computational requirements and sensitivity to duct diffuser angles are then explored in Sections 5.3–5.6.

5.1. Validation and implementation of the BEMT method

It is seen that converged axial induction levels are below the transition to the highly loaded regime for the majority of calculations, except at the blade tips and at high TSRs outside of the optimal

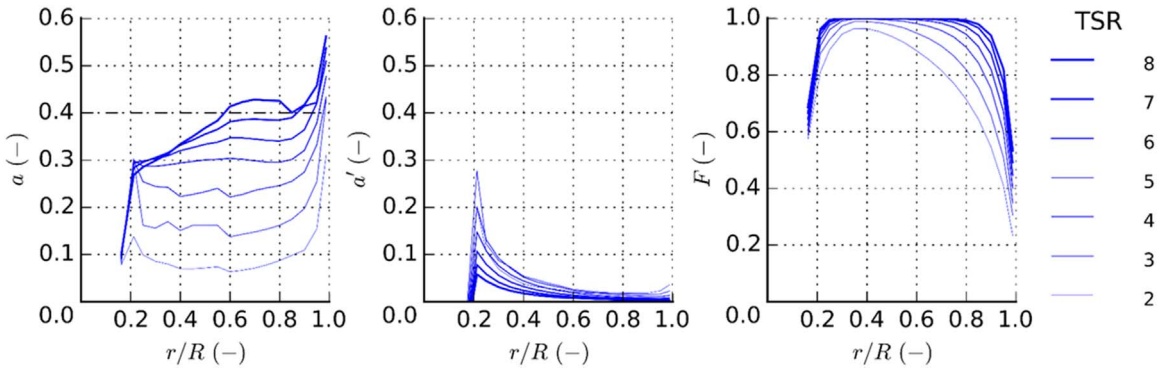

Fig. 4-1. a) axial induction factor (left), b) tangential induction factor (middle) and c) tip/hub correction factor (right) variation with normalised radius at various tip speed ratios, for inflow of 1.73 m s^{-1}, pitch 5, taken at an azimuth of 0°.

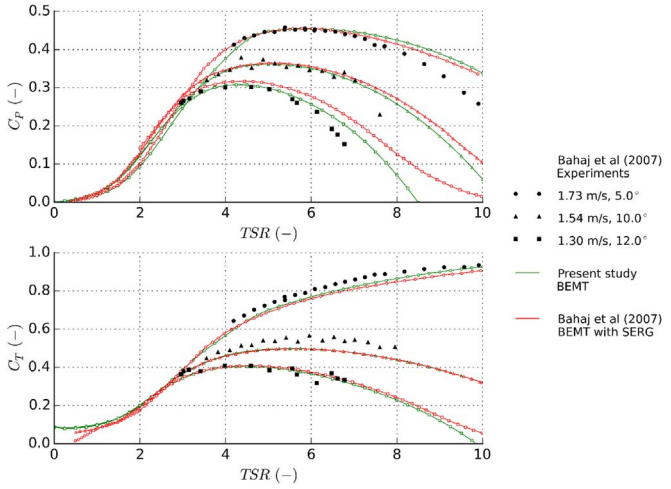

Fig. 4-2. Coefficient of power (top) and thrust (bottom) variation with tip speed ratio for 1/20th scale classical bare turbine for velocities and blade pitches: 1.73 m s^{-1}, 5°; 1.54 m s^{-1}, 10°; and 1.3 m s^{-1}, 12°. Comparing experimental data with BEMT results from present study and with University of Southampton (SERG).

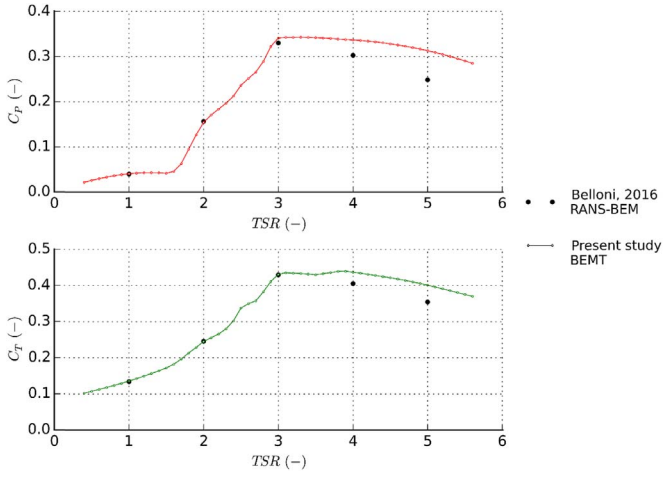

Fig. 4-3. a) coefficient of power (top) and b) thrust (bottom) variation with tip speed ratio for full scale open centre and ducted turbine, comparing present ducted BEMT with RANS-BEM results.

operating conditions. Intermediate calculations of flow parameters show that convergence is fully established within the model limits for each simulation.

The comparison of the classical BEMT model with the University of Southampton model (SERG) results shows that the developed code presented here achieves a good implementation of the theory. The

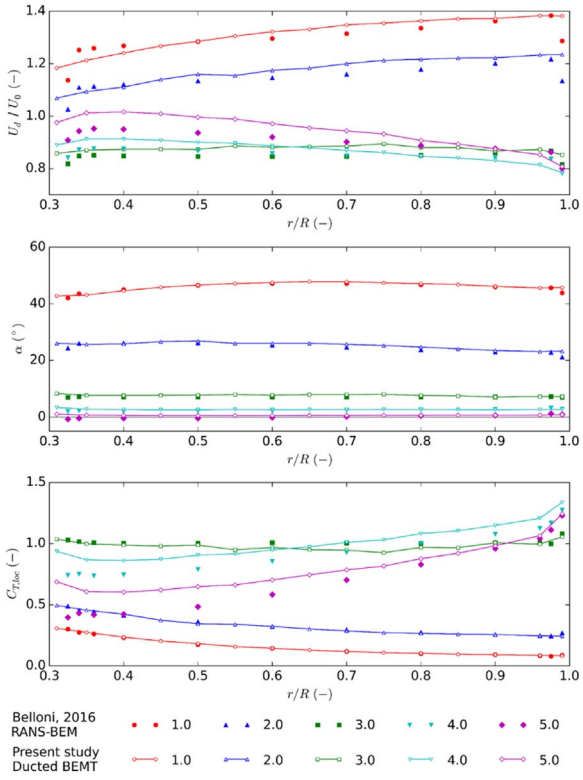

Fig. 4-4. Variations of a) flow velocity at the disc divided by velocity at the inlet (top), b) angle of attack (middle) and c) local elemental thrust coefficient (bottom) with normalised radius for various tip speed ratios, comparing ducted BEMT (lines) with RANS-BEM (points).

models also show very good agreement with the experimental measurements of C_P and C_T, with a slight tendency to over predict at higher TSR values. This is thought to be accounted for by the blockage effects within the experimental set up. In engineering applications, these TSRs are of less interest as they exceed the optimal operating conditions of the turbine. Further validation of the code is carried out against additional experiments and are detailed in Allsop et al. (2016).

5.2. Ducted BEMT comparison with RANS BEM

The overall values of rotor C_P and C_T are almost identical for TSRs below 4, which include the optimal operating conditions.

Both methodologies make use of the blade element theory, using similar geometrical parameters, aerofoil lift and drag coefficients and correction factors. The differences in the results from the two studies are therefore purely a function of how the changes in fluid momentum are treated. As there is good agreement seen between the results, the

suggestion is that the momentum changes calculated within the analytical ducted BEMT are very similar to those computed by the CFD model. Further analysis of the radial distributions indicate the calculations are similar on an elemental level and not only rotor averaged. Although this has positive implications for the approach taken, this is not a comprehensive validation of the method and more representative of an early stage qualification. In order to increase confidence in the method, further comparisons are recommended ideally against higher fidelity blade resolved CFD.

Over predictions seen at higher TSRs are likely due to the more complex flow characteristics at these conditions, which are better captured using the more detailed CFD. Assessment of the blade distributions shows that the over predictions of disc velocity are located closer to the hub, with the tips shows more reasonable correlation. This is thought to stem from flow interactions with the hub, with fluid likely being drawn through the open-centre and therefore reducing the hydrodynamic efficiency of the blade elements towards this region. As the model does not account for span wise flow, the application of a hub-loss factor could be considered, based on further analysis of these interactions.

5.3. Additional observations

Axial induction factors converge on values less than the transition point to the highly loaded regime, therefore under the input conditions considered, the results are always solved as per the ducted BEMT calculations. This shows a non-dependency on the Buhl correction factor, which has associated uncertainties due to semi-empirical nature of the correction based on experiments with a significant spread.

In order to remain consistent with the inputs of the RANS-BEM model, the lift and drag coefficients at angles of attack above 35° are kept constant with the reason being that this is a rare occurrence at non-optimal operating conditions. It is seen that for low TSR, the angles of attack are consistently above this limit, and therefore a post stall model could be used such as the Viterna extrapolation function which is commonly employed, in order to improve the accuracy of the aerodynamic coefficients.

5.4. Computational requirements

Studies on conventional turbines quoted computational requirement of 100 CPU-hours per turbine rotation using blade resolved RANS CFD and 12 CPU-hours for each simulation using coupled RANS-BEM (McIntosh et al., 2012). No details on the computational set up is given by this reference.

The coupled RANS-BEM study was performed on a 16 node computer cluster, with 8 cores per node. Steady computations were completed in 8 hours using 4 cores, equivalent to 32 core hours for each of the 5 simulations (Belloni, 2013).

The present ducted BEMT computations were performed using a laptop running an *Intel Core™ i5* 2.9 GHz dual core processor with 8 GB RAM. Simulations were completed within 3 min, generating all 60 points on the power and thrust curves, equivalent to 6 core minutes. Computational time from separate studies cannot be directly compared, due to dependencies on factors such as the computer used, processor type, number of partitions and clock time. There are also dependencies on certain CFD parameters such as the mesh definition, domain size and time step used. However, differences of several orders of magnitude seen in this study is indicative of substantial computational cost savings when using the current model. This highlights an advantage in the application of performing engineering assessments such as fatigue damage or when making multiple design iterations.

5.5. Model limitations

Both the ducted BEMT and RANS BEM models are based on the blade element theory restrictions, where any span wise flow is not considered, and individual aerofoil sections are analysed as a function of the lift and drag coefficients. In order to reduce the limitations of 2D analyses, corrections for physical behaviour could be included, such as the delayed stall effects by applying the Du-Selig and Eggers adjustments to lift and drag coefficients. However, the complex flow through the different turbine configuration is likely to have impacts on the Coriolis Effects of flow, and would need to be further analysed.

RANS has the ability to capture the spanwise flow, however this is beyond the capabilities of the momentum equations which are based on independent annular rings, capturing no radial interactions between elements. This is thought to be more significant around the open centre hub geometry. As the bending stress is a function of all forces along the blade, this is thought to have implications on blade life, and should be considered when feeding the loads into a structural analysis.

The incorporation of the duct effects in the BEMT equations are devised from CFD studies of unidirectional duct geometries. When applying this to the bi-directional duct in this case, the inlet and outlet angles are less easy to define, yet are incorporated within the empirical expressions. These angles were empirically calibrated using a separate study on an open centre device, comparing the resultant C_P and C_T curves with blade resolved CFD studies. There are inevitably inaccuracies with this approach due to the differences in the geometry of machines, as well as calibrating against a methodology that models individual blades.

The BEMT model is unable to characterise the flow in the wake, and does not consider any mixing with the fluid surrounding the stream tube. The present study only considers a flow direction perpendicular to the rotor plane, however this could be adapted to additionally assess yaw. The flow is also considered inviscid and steady and therefore does not account for dynamic effects such as turbulence or inertia. Quasi static simulations can be performed, where frozen inflow conditions are applied at each time step.

5.6. Sensitivity to duct model parameters

Additional simulations were performed in order to assess the effect of adding the duct correction, as well as the impact the diffuser parameters has on the power and thrust predictions. Fig. 5-1 shows that the classical BEMT results are lower than those predicted by the ducted BEMT for the majority of TSRs, as expected due to the flow augmentation effects. Additionally, various duct parameters are tested, using: $\theta_{in} = 0°/\theta_{out} = 0°$ (as a low extreme), $\theta_{in} = 30°/\theta_{out} = 10°$ (as the reference values from a calibration study) and $\theta_{in} = 60°/\theta_{out} = 20°$ (as a

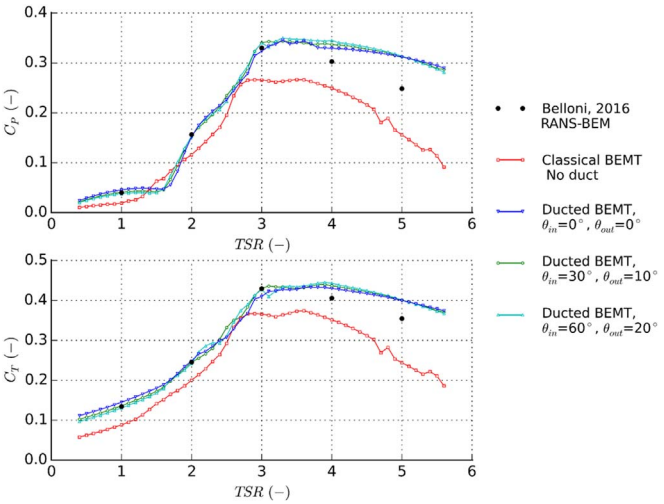

Fig. 5-1. a) coefficient of power (top) and b) thrust (bottom) variation with tip speed ratio for full scale open centre and ducted turbine, comparing classical BEMT with Ducted BEMT with various diffuser parameters.

high extreme of twice the reference values from a calibration study). It can be seen that power and thrust predictions using extreme values are within 5% of those when using the reference in this study, indicating a small sensitivity to these parameters.

6. Conclusion

This study details a 'classical' BEMT model, developed for analysing power output and rotor thrust forces on 3-bladed, bare TSTs. The developed BEMT code is implemented and verified by comparing results to an academic code and proves being capable of representing physical effects with good agreement to scale model experimental measurements.

An analytical model which aims to characterise the effects of flow through a duct as a function of the inlet efficiency, diffuser efficiency and base pressure is considered. Empirical expressions for these parameters are formulated in the literature, based on CFD studies of various different unidirectional ducts, as functions of numerical coefficients and duct geometry. The empirical expressions are combined to formulate a new expression for the axial induction factor, which is incorporated into the BEMT iterative procedure. Due to the geometrical differences of a bidirectional duct, certain values are calibrated through applying the model using blade resolved CFD results.

The rotor power and thrust predicted by the ducted BEMT model is almost identical to a RANS BEM study, for TSRs up to the optimal operating condition. As the blade element theory application is consistent in each method, this suggests a similar computation of the momentum change from the empirical expression and the CFD. This is further emphasised by similarities seen in the blade distribution of flow velocity, angle of attack and local elemental thrust.

Some divergence is seen at higher TSRs, with differences up to 25% higher power and 13% higher thrust compared to RANS BEM. These are a result of over predictions in the elemental flow velocity close to the hub, thought to be due to the flow around the hub and through the open centre, which are beyond the capability of the BEMT method to capture. A hub loss factor could be introduced to approximate the reduced hydrodynamic efficiency in this region, however would require detailed CFD analysis to ensure the complex flow interactions are well represented.

The ducted BEMT has shown significantly lower computational requirements compared with the coupled RANS BEM method, in the order of a few minutes on a laptop rather than a few hours on a computer cluster. This highlights the advantage of the model when multiple engineering assessments are required in performing fatigue analyses, or when access to high performance/clustered computational resources are restricted.

Despite the positive implications of these results, it should be noted that this study is not a comprehensive validation of the method. Due to the limited number of data points for comparison, this result is more representative only of an early stage qualification. Assessment against additional cases, preferably with alternative models or experimental measurements should be performed to form a more definitive conclusion.

As further and ongoing work, the presented model is being applied to commercial turbines, for further validation against blade resolved CFD studies under several inflow velocities. Sensitivity studies will also be performed on other duct parameters such as the inlet and diffuser ratios, to gain a better understanding of the model dependencies. The model will then be extended to calculate the associated stress distributions along the blade. The fast computation of this method will enable a higher number of analyses to be performed with many different inflow parameters, and ultimately used to predict blade fatigue damage.

Acknowledgments

This research is carried out as part of the Industrial Doctoral Centre for Offshore Renewable Energy (IDCORE) programme, funded by the Energy Technology partnership and the RCUK Energy programme (Grant number EP/J500847/1), in collaboration with EDF R & D. The authors would also like to thank Optydro for supplying blade resolved CFD results, in order to calibrate the duct model.

References

Abbott, I.H., Von Doenhoff, A.E., 1959. Theory of Wing Sections (Including a Summary of AirfoilData). Dover Publications Inc, New York, Langley, (Available at)⟨http://www.journals.uchicago.edu/doi/10.1086/470266⟩.

Allsop, S., et al., 2016. A validated BEM model to analyse hydrodynamic loading on tidal stream turbine blades. In: Proceedings of the 3rd Asian Wave and Tidal Energy Conference, 24–28 October 2016. Singapore.

Bahaj, A.S., et al., 2007. Power and thrust measurements of marine current turbines under various hydrodynamic flow conditions in a cavitation tunnel and a towing tank. Renew. Energy 32 (3), 407–426.

Batten, W.M.J., et al., 2006. Hydrodynamics of marine current turbines. Renew. Energy 31 (2), 249–256.

Batten, W.M.J., et al., 2007. Experimentally validated numerical method for the hydrodynamic design of horizontal axis tidal turbines. Ocean Eng. 34 (7), 1013–1020.

Belloni, C., 2013. Hydrodynamics of Ducted and Open-Centre Tidal Turbines (Ph.D. Thesis). The University of Oxfordhttp://www.eng.ox.ac.uk/civil/publications/theses/belloni.

Belloni, C., Willden, R.H.J., Houlsby, G., 2016. An investigation of ducted and open-centre tidal turbines employing CFD-embedded BEM. Renew. Energy.

Buhl, M.L., 2005. A New Empirical Relationship between Thrust Coefficient and Induction Factor for the Turbulent Windmill State.

Burton, T., et al., 2011. Wind Energy Handbook 2nd ed.. John Wiley & Sons Ltd, Chichester, UK.

van Bussel, G.J.W., 2007. The science of making more torque from wind: Diffuser experiments and theory revisited. J. Phys.: Conf. Ser. 75, 12010.

Chapman, J.C., et al., 2013. The Buhl correction factor applied to high induction conditions for tidal stream turbines. Renew. Energy 60, 472–480. http://dx.doi.org/10.1016/j.renene.2013.05.018.

DNV GL Garrad Hassan, 2012. Tidal Bladed Theory Manual.

Drela, M., 1989. XFOIL: an analysis and design system for low Reynolds number airfoils. Low Reynolds number aerodynamics, volume 54, pp 1–12. Available at: ⟨http://link.springer.com/chapter/10.1007/978-3-642-84010-4_1⟩.

Fleming, C., McIntosh, S.C., Willden, R.H.J., 2011. PerAWaT Report: WG3 WP1 D2 Model setup for ducted horizontal axis flow turbines.

Fleming, C.F., Willden, R.H.J., 2016. Analysis of bi-directional ducted tidal turbine performance. Int. J. Mar. Energy 16, 162–173.

Fuglsang, P., Dahl, K., Antoniou, I., 1999. Wind tunnel tests of the Risø-A1-18, Risø-A1-21 and Risø-A1-24 airfoils, Roskilde, Denmark.

Hansen, 2004. AirfoilPrep excel instructions.

Hansen, M.O.L., 2008. Aerodynamics of Wind Turbines Second. Earthscan, London, UK.

Lawn, C.J., 2003. Optimization of the power output from ducted turbines. Proc. Inst. Mech. Eng. Part A: J. Power Energy 217 (2002), 107–117.

Masters, I., et al., 2011. A robust blade element theory model for tidal stream turbines including tip and hub loss corrections. J. Mar. Eng. Technol. 10 (1), 25–35.

McIntosh, S.C., Fleming, C., Willden, R.H.J., 2012. PerAWaT Report WG3 WP1 D3: Performance and wake structure of a model horizontal axis axial flow turbine.

MeyGen, 2016. No Title. Project Update Spring 2016. Available at: ⟨http://www.meygen.com/wp-content/uploads/Meygen-Newsletter-201602.pdf⟩.

Moriarty, P.J., Hansen, aC., 2005. AeroDyn Theory Manual, Available at: ⟨http://www.nrel.gov/docs/fy05osti/36881.pdf⟩.

Ning, S.A., 2013. AirfoilPrep documentation, Technical Report NREL/TP-5000-58817 (release 0.1.0).

ReNews, 2016. No Title. Atlantis to decommission SeaGen. Available at: ⟨http://renews.biz/101295/atlantis-to-decommission-seagen/⟩.

SciPy Community, 2016. SciPy reference guide. SciPy reference guide v0.18.1. Available at: ⟨https://docs.scipy.org/doc/scipy-0.18.1/reference/index.html⟩.

Shives, M., 2011. Hydrodynamic Modeling, Optimization and Performance Assessment for Ducted and Non-ducted Tidal Turbines. Available at: ⟨http://dspace.library.uvic.ca:8080/handle/1828/3801⟩.

Shives, M., Crawford, C., 2011. Developing an empirical model for ducted tidal turbine performance using numerical simulation results. Proc. Inst. Mech. Eng. Part A: J. Power Energy 226 (1), 112–125 , (Available at)⟨http://pia.sagepub.com/content/226/1/112.abstract⟩.

Tangler, J.L., Selig, M.S., 1997. An Evaluation of an Empirical Model for Stall Delay due to Rotation for HAWTS. Windpower'97.

Turnock, S.R., et al., 2011. Modelling tidal current turbine wakes using a coupled RANS-BEMT approach as a tool for analysing power capture of arrays of turbines. Ocean Eng. 38 (11–12), 1300–1307 , (Available at)http://dx.doi.org/10.1016/j.oceaneng.2011.05.018.

UIUC Applied Aerodynamics Group, 2015. UIUC Airfoil Coordinates Database. Available at: ⟨http://m-selig.ae.illinois.edu/ads/coord_database.html⟩ (Accessed 25 February2015).

Viterna, L.A., Janetzke, D.C., 1982. Theoretical and experimental power from large horizontal-axis wind turbines.